

# EVALUATION OF ACOUSTIC SNAPSHOT ARRAYS FOR ROTORCRAFT SOURCE NOISE CHARACTERIZATION

James H. Stephenson  
*U.S. Army Combat Capabilities Development Command  
Aviation & Missile Center  
Hampton, VA, USA*

Mary L. Houston  
*Analytical Mechanics Associates, Inc.  
Hampton, VA, USA*

Historical development of acoustic hemispheres has required steady flight of a rotorcraft vehicle across a large linear array of microphones. The US Army, NASA, and Navy recently conducted a rotorcraft acoustics flight test in which multiple “snapshot” microphone arrays were used alongside a traditional linear microphone array. The snapshot arrays allow for a near instantaneous capture of rotorcraft acoustic emissions, without the need for steady flight. Development of the snapshot array is contained herein, and an evaluation of effectiveness of the array during adverse weather conditions. The snapshot arrays captured significant variation in acoustic emissions throughout a single run and between multiple runs of similar conditions. Hemispheres were created and modelled in land-use planning software and an investigation of A-weighted Sound Exposure Level (SEL [dBA]) was conducted. Sideline predictions of SEL compared well (within 0.1 dBA) between traditional and snapshot arrays, while centre line locations were less favourable with a difference of 1.6 dBA. Future refinement is required for the snapshot array technique, including advanced design of microphone placement and employing a semiempirical method to interpolate between measurement points, instead of the linear frequency weighting conventionally employed.

## 1. INTRODUCTION

Acoustic emissions of rotorcraft vehicles are a critical concern to the design of new aircraft, such as those in development under the Future Vertical Lift program, and to the future of Urban Air Mobility (UAM)<sup>[1–4]</sup>. Once a new rotorcraft is produced, it goes through acoustic emission experiments that measure the noise the vehicle produces in multiple directions. This information is then used to assess whether the new vehicle conforms to acoustic performance and certification requirements, but also can provide the basis for land-use modelling and community noise reduction of the vehicle<sup>[5]</sup>.

Significant work has been accomplished in rotorcraft acoustics modelling in recent years<sup>[6,7]</sup>, with much of the work turning towards manoeuvring flight<sup>[8–18]</sup>. Historically, rotorcraft acoustic emissions were measured by flying a vehicle in steady-state over a linear array of microphones. As the vehicle passed over the array of microphones, acoustic data were measured for different presentation angles. This allowed for a vehicle-centred noise hemisphere to be constructed<sup>[19]</sup>. Acoustic data were captured on the traditional linear array within  $\pm 610$  metres from the reference location, and so this steady-state condition

must be maintained for up to 40 or more seconds, depending on vehicle speed.

The true requirement is that the aerodynamic conditions through the rotor system that are producing the measured noise must be maintained, so that at each time stamp (and therefore each measured presentation angle) the microphones are measuring the same acoustic phenomena. However, there are over 600 aerodynamically complex vehicles under development for the Urban Air Mobility market and Future Vertical Lift program that have multiple independently controlled rotor systems and auxiliary lift and control surfaces<sup>[3]</sup>. These vehicles generally have fly-by-wire piloting systems, which actively trim the vehicle by varying rotor state conditions and control surfaces. Thus, it cannot be assumed that future vehicles will be able to maintain an aerodynamically constant condition through the rotor system across a full acoustic run<sup>[20]</sup>.

Previous experiments have employed two-dimensional arrays in an effort to capture impulsive acoustic emissions caused by manoeuvring flight<sup>[10,13,16,17,21]</sup>. These works, however, were not intended for land-use modelling efforts and so appropriate hemispheres of data were not developed and evaluated. In the current experiment, a “snapshot” array was developed to create instantaneous hemispheres for predictions with land-use planning models such as the Advanced Acoustic Model<sup>[22]</sup>. The guiding principals of the array design were to

---

This is a work of the U.S. Government and is not subject to copyright protection in the U.S. DISTRIBUTION STATEMENT A. Approved for public release.

adequately capture a full hemisphere at a single instant in time, with sufficient emission coverage to be employed in land-use planning models, while minimizing the total number of microphones required.

The effectiveness of the snapshot arrays will be evaluated by comparing spectral content from multiple snapshot hemispheres of similar conditions, as well as comparing snapshot array hemispheres to those built using a traditional linear array. Additionally, Sound Exposure Level (SEL) predictions for both the snapshot and traditional arrays will be compared at locations used in certification of new vehicles to determine if the snapshot technique is applicable to modelling community noise impacts.

The data used in the following analysis were acquired during a joint flight test looking into the acoustic emissions of an MD530 helicopter, conducted by the US Army, NASA, and US Navy<sup>[23]</sup>. Relevant portions of the flight test are documented here, along with the development of the array and evaluation results. A complimentary technical memorandum<sup>[23]</sup> has been published, which fully documents the equipment used, data acquired, and the availability of the data.

## 2. TEST DESCRIPTION

### 2.1 Vehicle Specifications

This test was conducted in Yuma, Arizona with an MD530 rotorcraft, shown in Figure 1. The MD530 is a light-utility civilian vehicle with a single Rolls-Royce 250-C30 engine. The vehicle has an 8.38 metre (27.5 foot) diameter, 5-bladed main rotor system, with a two bladed tail rotor. The MD530 was tested for acoustic emissions as well as certification data, and has a main rotor blade passage frequency of 39.75 Hz and tail rotor blade passage frequency of 95 Hz. This vehicle was flown with ballast on-board to ensure sufficient weight during certification test points, and as such, had a take-off weight of 1520 kg (3350 lbs). Aircraft state data were measured with NASA's Aircraft Navigation and Tracking System (ANTS), and are provided in Table 1.

### 2.2 Microphone Specifications

The NASA Mobile Acoustics Facility (MAF) was used to acquire the acoustic data. This facility is comprised of a semi-trailer used as a command station from which to control the flight test as well as to maintain, store, and charge the 80 Wireless Acoustic Measurement System version II (WAMS II) units. Each WAMS II unit consists of a microphone, ground board, radio antenna, GPS receiver, and on-board SD card for data recording. The GPS receiver was used to obtain Coordinated Universal Time (UTC) stamps that



Fig. 1: MD530 vehicle in flight over test range.

synchronized all microphone, aircraft, and weather instrumentation.

During this test, the standard WAMS II setup consisted of a GRAS 67AX microphone embedded in a 381 mm (15 inch) diameter round ground board, as shown in Figure 2. Microphones are offset from the centre of the ground board to minimize edge effects. This microphone position and ground board configuration is based on the SAE Aerospace Recommended Practice ARP4055<sup>[24]</sup>. All microphones are sampled simultaneously and uninterrupted throughout a run at 25 kHz with 24-bit resolution. Up to 63 of these systems were deployed at one time for this flight test.



Fig. 2: WAMS II setup with GRAS 67AX microphone.

Microphones were deployed in four interlaced arrays, as shown in Figure 3. A Cartesian coordinate system is used to describe the location of the microphones with respect to the flight path. X is defined along the flight track and is positive in the primary flight direction; Y is defined perpendicular to the flight track and is positive to the aircraft port (left) side; Z

Table 1: MD530 vehicle state data variables from ANTS.

Variable Name	Description	Units
utcsec	UTC seconds after midnight	second
latitude	Current vehicle latitude	decimal degrees
longitude	Current vehicle longitude	decimal degrees
heading	Current vehicle heading relative to magnetic North	°
altitude	Current altitude	metre
x	Vehicle location in local 'X' coordinate	metre
y	Vehicle location in local 'Y' coordinate	metre
z	Vehicle location in local 'Z' coordinate	metre
velocity_down	Vehicle speed in down direction	metre/second
velocity_easting	Vehicle speed in East direction	metre/second
velocity_northing	Vehicle speed in North direction	metre/second
velocity_x	Vehicle speed in local 'X' direction	metre/second
velocity_y	Vehicle speed in local 'Y' direction	metre/second
velocity_z	Vehicle speed in local 'Z' direction	metre/second
acceleration_x	Vehicle acceleration in local 'X' direction	metre/second <sup>2</sup>
acceleration_y	Vehicle acceleration in local 'Y' direction	metre/second <sup>2</sup>
acceleration_z	Vehicle acceleration in local 'Z' direction	metre/second <sup>2</sup>
pitch	Vehicle pitch	°
roll	Vehicle roll	°

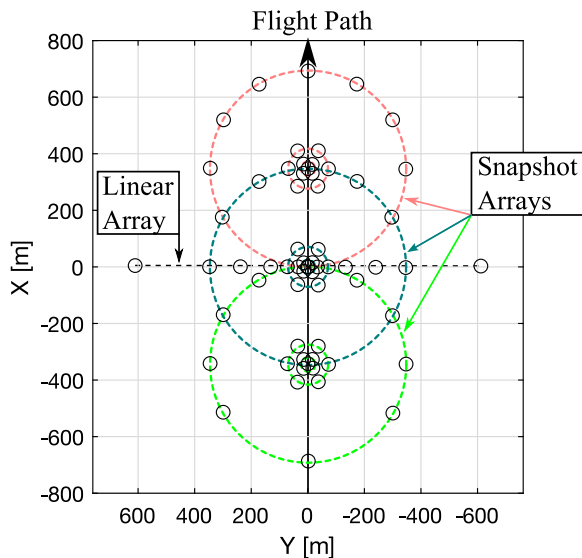


Fig. 3: Microphone locations with snapshot and linear arrays identified. Snapshot arrays are numbered in flight direction, such that Array 1 is centred at  $X = -345$  m, Array 2 is centred at  $X = 0$  m, and Array 3 is centred at  $X = 345$  m.

is positive up. Microphones were generally numbered sequentially from the negative to positive in the 'X' direction, and from positive to negative in the 'Y' direction, with microphone 31 defined as the centre of the coordinate system ( $X = Y = Z = 0$ ). Microphone 31 is also at the geometric centre of the overall microphone array, and is shared by all four individual arrays. Fig-

ure 4 is a satellite image with all equipment precisely

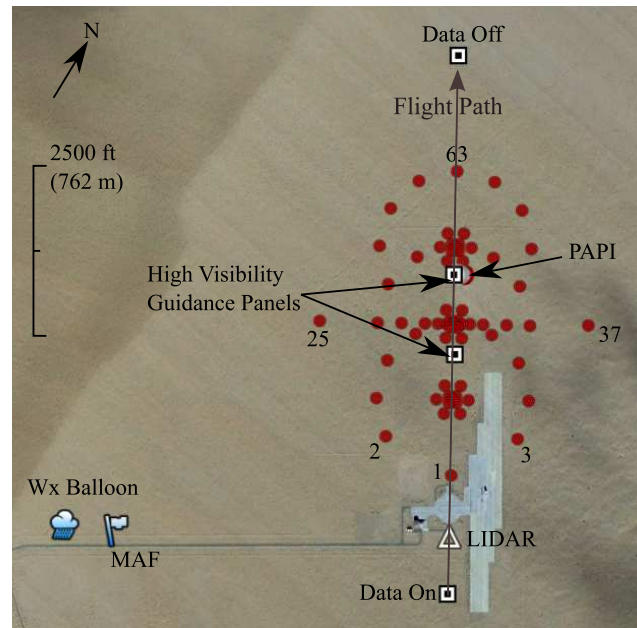


Fig. 4: Satellite photo of test location with equipment identified.

located and identified.

In Figure 4, 'Wx Balloon' shows the location of the weather balloon that was used during testing, 'MAF' is the location of the Mobile Acoustics Facility trailer, and 'LIDAR' is the location of the wind measurement system that sampled wind velocity up to 300 metres

above ground level. The 'PAPI' system is an adjustable light system used to guide pilots on steady approach conditions. More information on these systems can be found below and in the associated technical memorandum<sup>[23]</sup>.

There are three individual instances of a snapshot array, as identified in Figure 3 by their individual colours. Each snapshot array features three concentric circular patterns of microphones to capture an entire hemisphere at a single instant in time. Each of the three snapshot arrays consisted of 21 microphones. Figure 5 shows the ideal hemisphere coverage for a vehicle passing over the centre of one snapshot array at an altitude of 61 metres ( $Z = 61$  m, 200 ft). The figure shows the microphone locations (circles) on a Lambert projection, as a function of azimuth (counter-clockwise around the centre) and elevation (radially inward). Each circle indicates a single microphone location, while the filled circles indicate locations of specific interest discussed below. Azimuth rotates with the direction of the main rotor, where  $0^\circ$  is the tail,  $90^\circ$  is the right side of the vehicle, and so forth. Elevation starts at the horizon plane ( $0^\circ$ ) and decreases radially inwards, such that  $-90^\circ$  is directly beneath the vehicle. The arrays will be referred to in order, from bottom to top of Figure 4, such that Array 1 is the first array the pilot encounters on a run (light green), Array 2 is the middle array (teal), Array 3 is the last array the pilot encounters on a given run (pink).

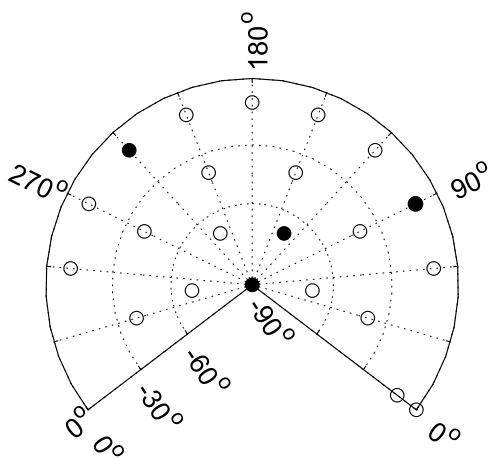


Fig. 5: Lambert projection of a single snapshot array. Circles indicate microphone locations with filled circles indicating directions of special interest used in further evaluation.

Each ring in the snapshot array shown in Figures 3 and 5 targets a specific elevation and azimuthal coverage. The outer ring had 10 microphones assigned to it, and was designed to capture near-horizon plane data at an elevation of  $-10^\circ$  and azimuthal spacing of approximately  $30^\circ$ . The elevation angle was chosen

as it is close to the horizon while allowing the ground board to minimize excess ground attenuation caused at grazing incidence angles<sup>[25]</sup>. The azimuthal spacing was chosen for the outer ring to be reasonably fine given the large area it must cover. The middle ring consisted of 6 microphones targeting  $-40^\circ$  elevation angle with an azimuthal spacing of  $60^\circ$ ; while the inner ring consisted of 4 microphones targeting  $-70^\circ$  elevation angle with an azimuthal spacing of  $90^\circ$ . The middle and inner rings are staggered azimuthally such that the area underneath the vehicle is adequately covered. Finally, the 21st microphone for each array was located directly underneath the vehicle at  $-90^\circ$  elevation.

This array spacing was hand-selected to minimize number of microphones and provide adequate hemispherical coverage. Proper optimization of microphone placement should be performed in the future to ensure uniform hemispherical coverage. Each of the snapshot arrays was deployed at 345 metre (1134 foot) intervals along the flight track so that microphone locations could be shared between arrays, minimizing overall microphone channel count. For instance, Microphone 31 is at an azimuth and elevation of ( $180^\circ, -10^\circ$ ) for Array 1, ( $90^\circ, -90^\circ$ ) for Array 2, and ( $0^\circ, -10^\circ$ ) for Array 3.

A traditional linear array was also deployed to capture a hemisphere of data for an entire flyover. The traditional linear array consisted of 13 microphones (numbered 25-37) deployed perpendicular to the nominal flight path, with microphone station 31 located on the flight trajectory. For this paper, microphones 19-41 were used to form the hemispheres in the 'linear' array and its coverage is shown in Figure 6, where each circle represents a half-second of data measured by each microphone in the array. The

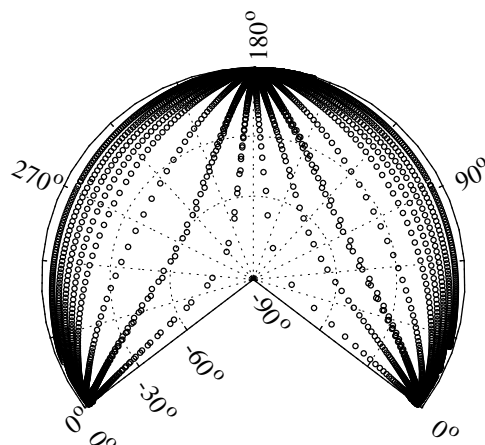


Fig. 6: Lambert projection of the linear array coverage.

additional microphones were within 64 metres (210

feet) in the flight direction of the intended linear array and allowed for a better coverage without requiring additional microphones on the traditional array. Comparing the traditional linear array coverage in Figure 6 to the snapshot array coverage in Figure 5, it can be seen that the snapshot array provides significantly less information for the generation of acoustic hemispheres.

While the traditional array provides substantially better hemispherical coverage than the snapshot arrays, recall that it requires the pilot and vehicle to maintain a steady flight condition across the entire run because data from different presentation angles are measured at unique times throughout the run. However, with the focus turning towards manoeuvring flight, as well as to complex vehicle configurations for which the ability to maintain a steady flight condition is uncertain<sup>[20]</sup>, it became necessary to develop a new method for characterizing the acoustic emissions of a vehicle in dynamic flight. The combination of four arrays deployed here allows for an interrogation into the steadiness of traditional rotorcraft noise throughout a single nominal flight condition and across multiple runs of nominally the same flight condition. Further, it sets the groundwork for future array development that can more adequately address the complex aeroacoustic emissions anticipated from future vehicles.

### 2.3 Weather Instrumentation

An extensive set of weather measurements were collected throughout the test. A tethered weather balloon system was located near the control trailer sufficiently far away from the flight path to not interfere with aircraft operations. The balloon altitude was fixed such that the balloon weather sonde was initially at 152 metres (500 feet) above ground level, although balloon altitude fluctuated throughout the day due to variation in wind speed. A temperature profile was simultaneously measured using a temperature string built by RST Instruments Ltd. The temperature string was hung below the weather sonde and has sensors every 3 metres (10 feet) of tether, with a quoted accuracy of  $\pm 0.07^{\circ}\text{C}$ . These sensors recorded temperature as function of time, with the deployed sensors acquiring samples every 1-2 minutes.

A ZephIR 300 portable IEC 60825-1 Class 1 eye-safe LIDAR system was also deployed during testing. The LIDAR system was placed along the flight line and measured wind speed and direction at 12 altitudes up to 300 metres (984 feet) above ground level. The LIDAR has a wind speed range up to 80 m/s with accuracy of 0.1 m/s and direction variation of less than  $0.5^{\circ}$ . Additionally, six ground weather stations that measured wind speed, wind direction, pressure, temperature and humidity were placed around

the test site. Five sensors were mounted on 2-metre tripods, located near microphones 1, 25, 31, 37, and 63. The last station was mounted approximately 10 metres (33 feet) above ground level at the MAF.

### 2.4 Flight Test Manoeuvre Descriptions

Level flyover test conditions and approach points were measured with the MD530 vehicle. Level flyovers were flown at an altitude of 61 metres ( $Z = 61\text{ m}$ , 200 ft) AGL at the reference microphone location. The aircraft was flown in a steady-state condition throughout the duration of acoustic data acquisition at the prescribed airspeed and along the nominal flight path. For all level flyovers, data-on and data-off were called 1219 metres ( $X = \pm 1219\text{ m}$ , 4000 ft) before and after the reference microphone, respectively.

Approach test point conditions were also acquired. All approaches begin with the pilot acquiring the prescribed flight path angle (FPA) and airspeed at a sufficient range to be in a steady-state operating condition when crossing the data-on location. The glide slope intersected the ground at the location of a Precision Approach Path Indicator (PAPI) system, located 229 metres (750 feet) after the reference microphone ( $X = 229\text{ m}$ ). This steady-state approach condition was held for as long as possible throughout the descent to the PAPI, pulling out at the lowest possible altitude for safe flight operations. A 15 metre ( $Z = 15\text{ m}$ , 50 ft) hard deck was implemented and followed by the pilots.

## 3. DATA PROCESSING PROCEDURES

### 3.1 Acoustic Data Post-Processing

Spectral calculations of the measured time-histories of each microphone were calculated using a Hamming window on 1/2-second intervals. Hemispheres were created by interpolating measured spectral amplitudes onto a uniform grid according to the Acoustic Repropagation Technique method used in the Advanced Acoustic Model<sup>[26]</sup>. The interpolation method used was Shepherd's modified inverse distance weighting with a 30 degree radius of influence<sup>[27]</sup>. Snapshot hemispheres used the 1/2-second of data when the vehicle passed closest to the centre microphone of each individual snapshot array, while the linear array used all data measured within 610 metres (2000 feet) from the centre microphone. Hemispheres of both narrowband and one-third octave band were created and analysed.

### 3.2 Vehicle Data Post-Processing

For this paper, only the level flyover conditions at a target speed of 120 knots true airspeed will be investigated. This condition has the most number of repeats

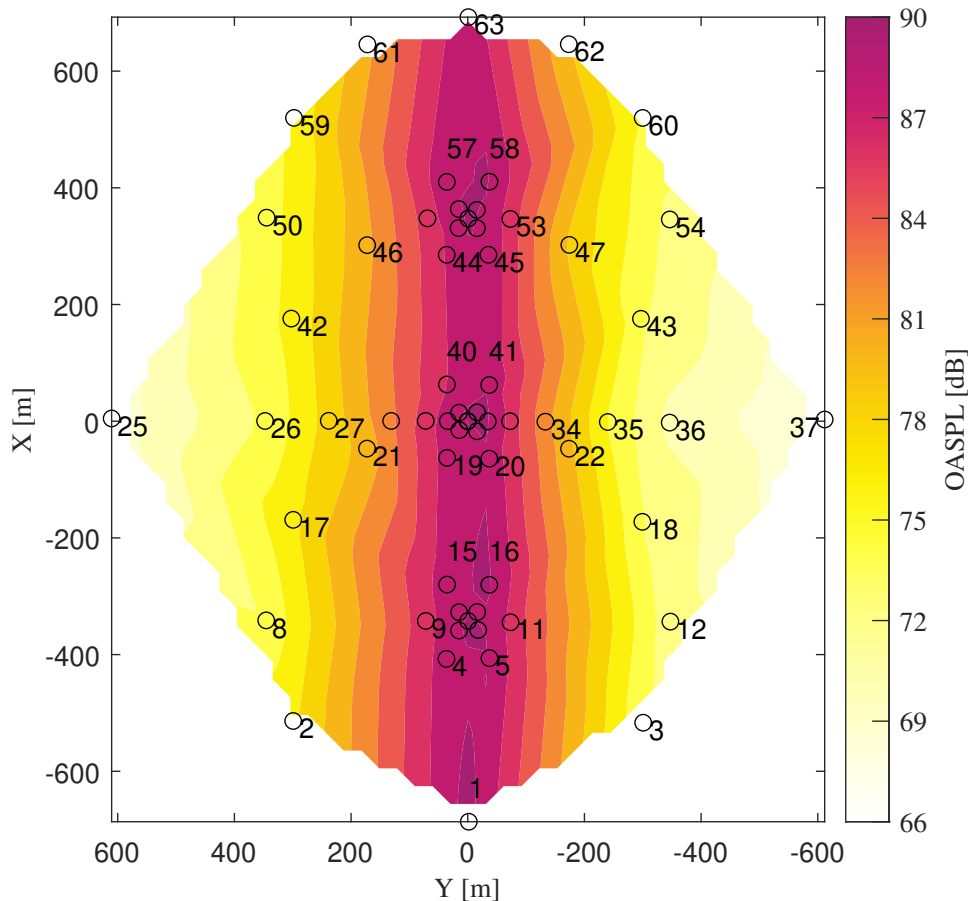


Fig. 7: Maximum Overall Sound Pressure Level [dB] for run 042420.

(eight) and allows for statistical analysis among the above mentioned microphone arrays. Details about the other flight conditions can be found in the technical memorandum<sup>[23]</sup>. True airspeed in the test condition flight direction was calculated by taking the headwind component of the LIDAR measured velocity at the flight altitude and adding it to the GPS recorded ground speed. Average true airspeed was  $115.8 \pm 3.3$  knots. For each of the runs, side winds were significant and varied from +8.6 knots (wind from pilot's right to left) to -4.7 knots (winds from pilot's left to right). It is anticipated that tail rotor acoustic emissions will be significantly impacted by the large and variable side winds. Overall, the eight runs investigated here have high wind speeds, ranging from 14.1 knots up to 22.2 knots. This magnitude and variation in wind speed and direction would typically be detrimental to quality data sets, but in this case it allows for an investigation in the robustness of these snapshot arrays under adverse conditions.

The vehicle's flight path angle and acceleration were also monitored throughout each of the individual runs. The flight path angle across the arrays for all runs averaged  $0.02^\circ \pm 0.23^\circ$ , while accelerations averaged  $0.02 \pm 0.02$  g. The plus/minus values pro-

vided for these two measurements are the maximum and minimum values the vehicle experienced, indicating that the pilot was able to hold the desired steady level flight condition, despite the adverse weather.

## 4. RESULTS

### 4.1 Individual Run Analysis

Figure 7 was created in order to develop an understanding of expected acoustic amplitudes for this vehicle. This figure shows the maximum overall sound pressure level measured by every microphone throughout one 120 knot flight across the test area. The numbered open circles identify each microphone location, while the colour provides the maximum overall sound pressure level measured throughout the run. The values of sound pressure level are only known at the microphone locations, so the contour plot is filled in using a linear interpolation scheme. The wind speed for this condition was 14.7 knots with a -0.8 knot side wind component. Figure 7 also shows microphones 19-41 numbered, which were used for the development of the traditional linear array. The overall sound pressure level contour plot shows anticipated trends, with the vehicle being louder near the flight

path and quieter off to the sides, with some slight hotspots appearing on the advancing side (right,  $-Y$ ).

More interestingly, snapshot hemispheres created for this particular run can be seen in Figure 8. A close investigation shows that the microphones (open circles) are not in the exact positions as designed in Figure 5 because the pilot was slightly off the desired flight track in the positive  $Y$  direction. The contour levels are set to 3dB increments, which accentuate differences among the hemispheres. Overall, first qualitative impressions of the hemisphere suggest reasonable agreement across the three snapshot hemispheres.

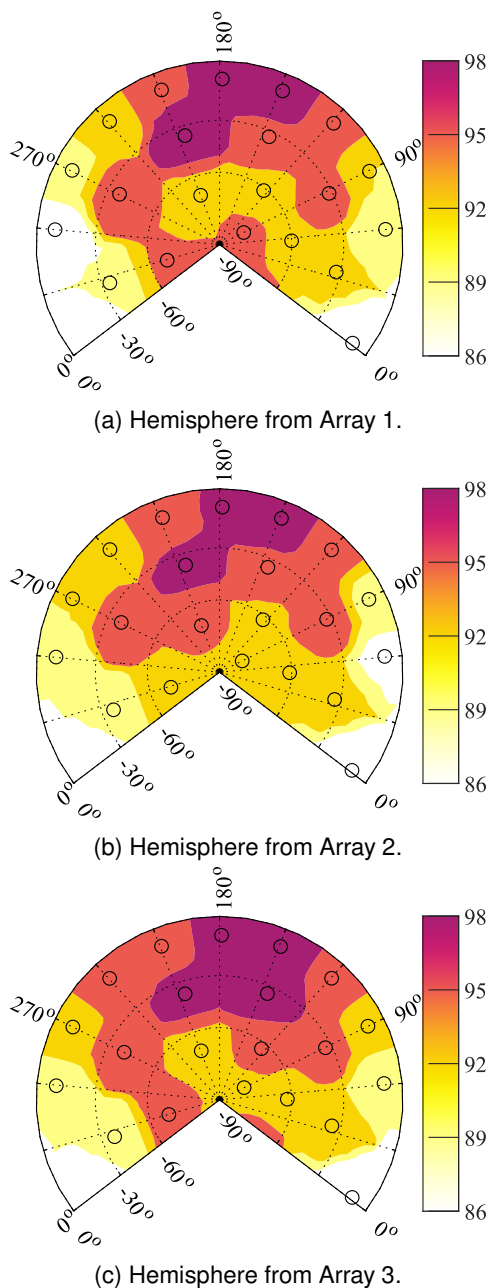


Fig. 8: Overall Sound Pressure Level [dB] of snapshot hemispheres from run 042420 seen in Figure 7.

Further investigation of the snapshot hemispheres is required to gain quantitative understanding of the snapshot capability. Four microphones are chosen for further investigation as they exhibit differing contour levels in the hemispheres from Figure 8. The four microphones chosen are marked in Figure 5 by their filled circle, and are located in azimuth and elevation directions of  $(90^\circ, -10^\circ)$ ,  $(240^\circ, -10^\circ)$ ,  $(135^\circ, -70^\circ)$ , and  $(90^\circ, -90^\circ)$ .

Figure 9 provides the narrowband spectra calculated for a single run at each of the four previously identified microphone locations for all three snapshot arrays. It can be seen that the tonal components of the spectra, those associated with the main rotor emissions (at multiples of 39.75 Hz) and tail rotor emissions (at multiples of 95 Hz), largely match among the three arrays for all four directions. The largest differences among the arrays are at frequencies between the dominant tonal peaks, which are likely driven by interplay and fluctuation of broadband noise components of the main and tail rotor systems, with some impact from the natural variation in ambient noise. This ‘noise’ in the spectra is exacerbated by investigating a single instance in time instead of averaging over multiple instances. This results in a larger measurement uncertainty in any individual frequency band, which is especially important for randomly generated noise such as rotor broadband noise.

One-third octave band spectra are also investigated for the same run, as integrating across the larger frequency widths allows for a reduction in the spectral uncertainty. Figure 10 provides these one-third octave band spectra. Figure 10a shows good agreement in the  $(90^\circ, -10^\circ)$  direction between one-third octave bands for the peak frequencies centred at 40 Hz and 200 Hz. At those frequencies, there is a 2.6 and 2.1 dB maximum difference among the three arrays, respectively. The 40 Hz centre frequency represents the first main rotor harmonic, while the 200 Hz frequency overlaps the fifth main rotor blade passage frequency harmonic and second tail rotor blade passage frequency harmonic. The 100 Hz centre third-octave band has a large 9.8 dB difference among the three arrays, but the peak value at that frequency is 4 dB below the lowest amplitude of the 40 or 200 Hz centre frequencies. This 100 Hz frequency band corresponds with the first tail rotor blade passage frequency harmonic. Recall, the tail rotor is susceptible to side winds, so this frequency in particular is anticipated to fluctuate among the arrays due to the substantial and variable side winds.

Figure 10b shows similar spectral amplitude spikes at 40 Hz and 200 Hz as was seen in Figure 10a. However, this microphone is located on the retreating side of the main rotor  $(240^\circ, -10^\circ)$  and so is subjected to significantly lower main rotor noise. Thus, the frequency spike at 200 Hz is close to 10 dB larger than

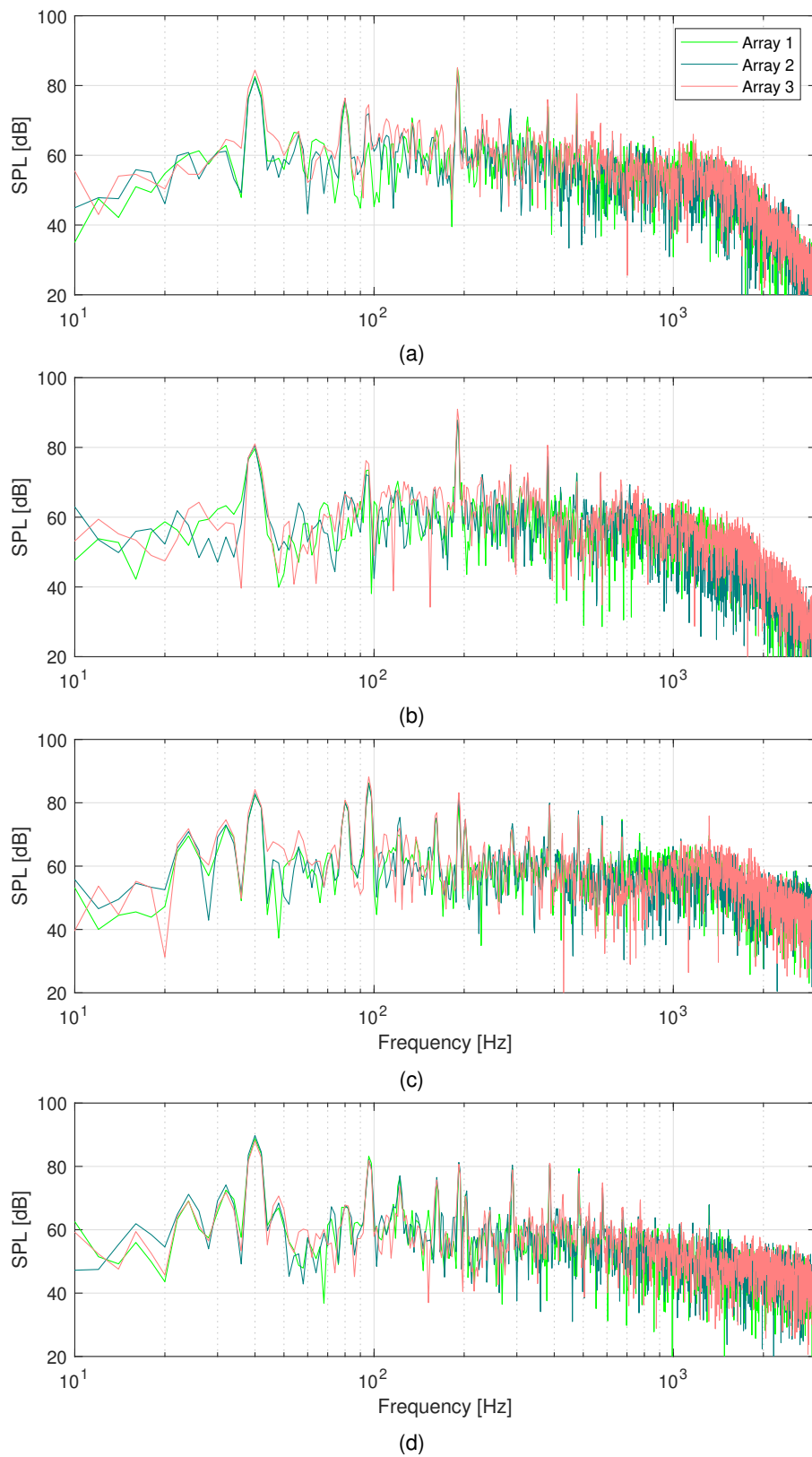
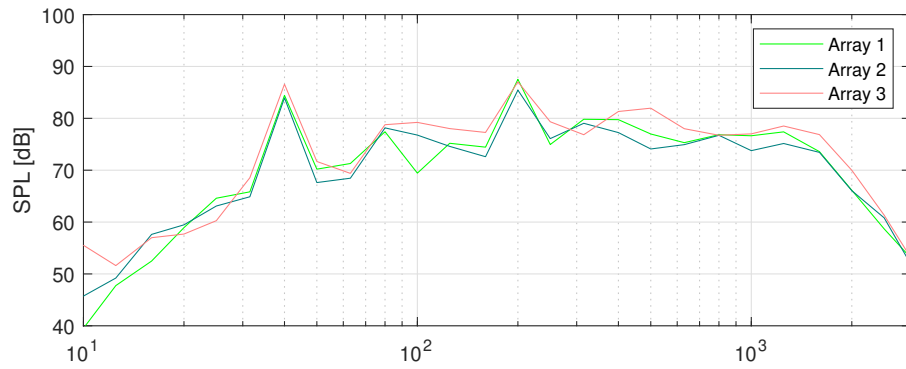
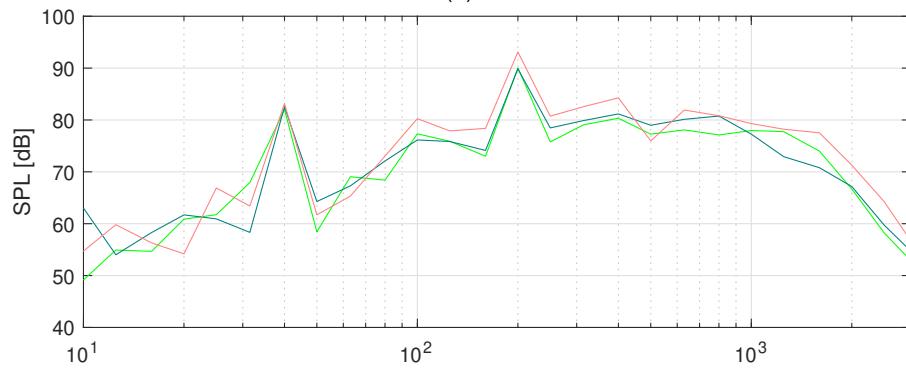


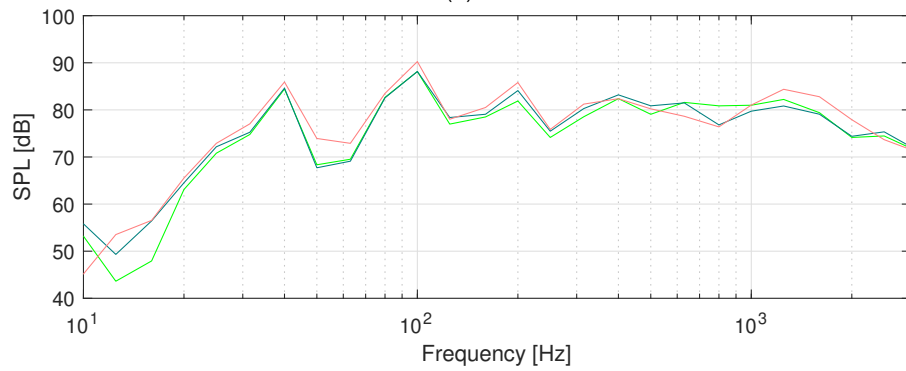
Fig. 9: Narrowband spectral levels of azimuth, elevation pairs from Figure 8 for (a) (90°, -10°), (b) (240°, -10°), (c) (135°, -70°) and (d) (90°, -90°).



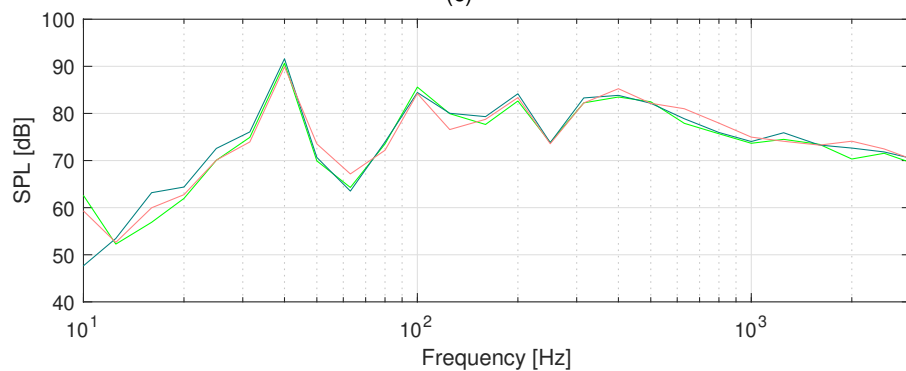
(a)



(b)



(c)



(d)

Fig. 10: One-third octave band spectral levels of azimuth, elevation pairs from Figure 8 for (a) (90°, -10°), (b) (240°, -10°), (c) (135°, -70°) and (d) (90°, -90°).

the spike at 40 Hz and has a 3.2 dB spread.

Figure 10c is from substantially below the rotor system at an azimuth of 135° and elevation angle of -70° degrees. This angle is dominated by loading noise with strong broadband noise components as well. In this direction, the one-third octave spectra among all three arrays compare very well. There are three potential peaks in the levels, one at 40 Hz, another at 100 Hz, and the final at 200 Hz. Among the three snapshot arrays, the amplitudes at these frequencies are within 1.3, 2.1, and 3.9 dB, respectively.

Finally, Figure 10d is from almost directly underneath the rotor system at a nominal elevation angle of -90° degrees, but actual angle of -82.6°. In this direction, the first main rotor harmonic dominates and compares well (within 1.7 dB) among arrays. The first tail rotor harmonic is 6 dB lower than the first main rotor harmonic and also agrees well (within 1.4 dB) among arrays.

Figure 10 shows the variation in acoustic emissions for similar directivities across a single run. However, there can be significant variations in emissions across multiple runs, especially due to the large variation in wind noise experienced. Figure 11 shows the one-third octave band spectra averaged in each similar direction across the three snapshot arrays, compared between the multiple runs of the same nominal condition. All eight runs are represented in the figure, from the same four directivities investigated previously. At the scale used, it appears that the amplitudes at the majority of the frequencies compare well, with the exception of some low frequency (less than 30 Hz) noise likely caused by wind, and higher frequencies (greater than 400 Hz) typically associated with broadband noise for level flyovers.

The vertical scale on Figure 11 is quite generous, with 10 dB tick marks, making it easy to see the all of the spectra, but difficult to determine important differences between runs. In order to alleviate this, Figure 12 was created to show the maximum difference between the runs for every one-third octave band centre frequency. This analysis requires careful evaluation, as large variations in amplitudes occur at frequencies with low overall amplitudes that do not significantly impact human perception. For instance, there is a larger than 25 dB difference at 10 Hz centre frequency for the 90° azimuth and -10° elevation direction. However, the 10 Hz bandwidth in Figure 10a is significantly lower in amplitude than the first main rotor harmonic at 40 Hz, so this large variation is insignificant.

Figure 12 should be investigated at the frequencies of maximum amplitudes in the signals shown in Figure 11. Prime frequencies for investigation are 40, 100, and 200 Hz, which correspond with the first main rotor and first two tail rotor harmonics. Fig-

ure 12 shows these values have a 3-5 dB difference between the runs, which can result in a substantial impact to the overall signal. Broadband noise frequencies from 300-1000 Hz are also important, and this range shows a variation up to 8 dB. These higher frequencies are important for community noise metrics such as Sound Exposure Level, as the human ear is more sensitive in this range. Therefore, it is possible that the large fluctuation in amplitudes at these frequencies are important.

## 4.2 Land-Use Modelling Analysis

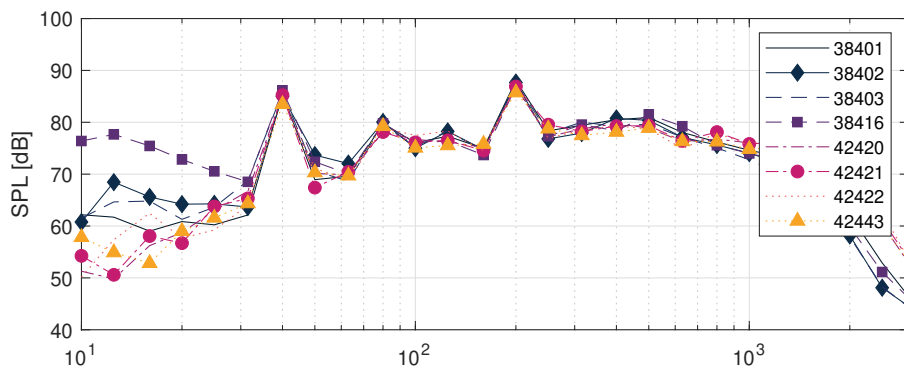
While it can be seen in Figures 8-10 that there are differences in spectral levels among the three arrays for a single run, and large fluctuations can be seen between runs in Figures 11 and 12, it remains unknown whether these fluctuations are typical and consistent with the data acquired for the traditional linear array hemispheres. Further, it remains unknown whether these differences are sizeable enough to result in changes to land-use modelling analysis, which may affect local flight restrictions or zoning decisions.

In order to investigate the effects of the snapshot arrays on land-use planning models, four hemispheres from each of the eight 120 knot runs were generated and virtually flown in the Advanced Acoustic Model. Three hemispheres were generated using the novel snapshot method, one from each of the snapshot arrays, and the fourth hemisphere was generated using the traditional linear array hemisphere method. These hemispheres were virtually flown at a test speed of 120 knots and an altitude of 150 metres (492 feet) above ground level. Three receiver locations were calculated, one to each side of the flight line at 150 metres (492 feet), and one directly beneath the flight track. These altitude and receiver positions mimic those required for vehicle type certification.

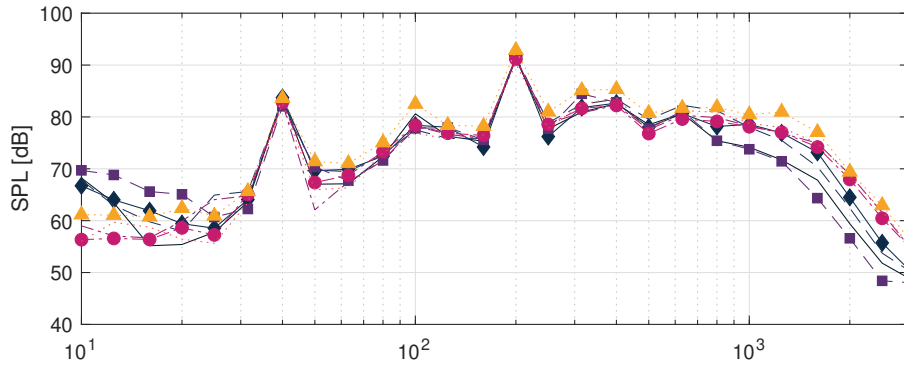
Table 2 shows the average and standard deviation of the A-weighted Sound Exposure Level (SEL [dBA]) for the three virtual microphones. The snapshot arrays have 24 individual models that went into the average (three arrays times eight runs), while the linear array has only eight individual models.

Table 2: Sound Exposure Levels [dBA] as predicted by the Advanced Acoustic Model for certification microphone locations. The plus/minus value provided is the standard deviation for that measurement.

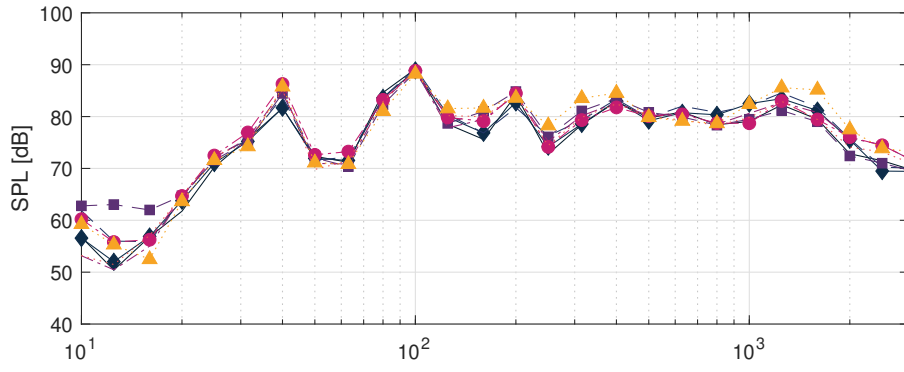
Array Type	Left Sideline	Centre	Right Sideline
Linear	82.5 ± 0.5	81.5 ± 0.4	82.7 ± 0.3
Snapshot	82.6 ± 0.6	83.1 ± 0.7	82.8 ± 0.3



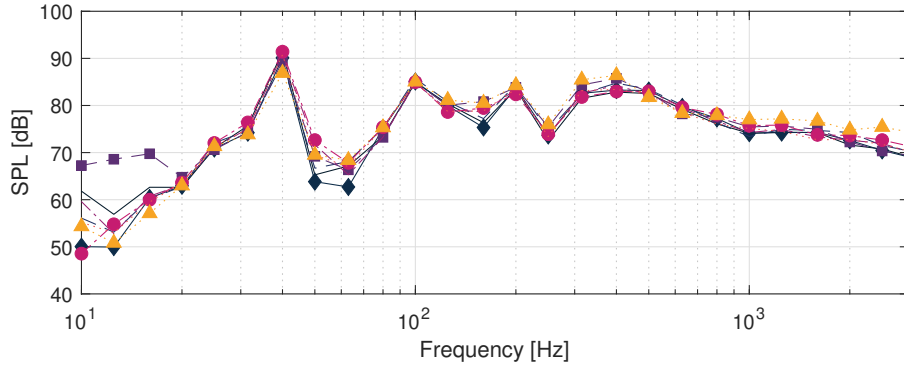
(a)



(b)



(c)



(d)

Fig. 11: Average one-third octave band spectral levels of azimuth, elevation pairs from Figure 8 for (a) (90°, -10°), (b) (240°, -10°), (c) (135°, -70°) and (d) (90°, -90°).

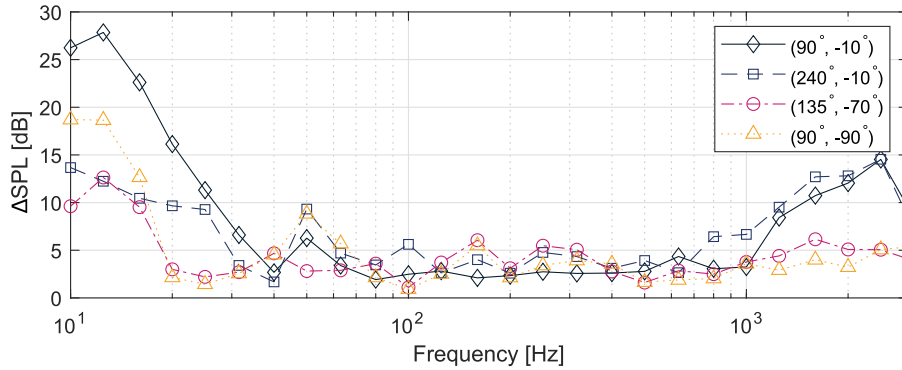


Fig. 12: Difference between the snapshot-averaged loudest and quietest one-third octave band levels across all runs for each directivity investigated previously.

It can be seen in Table 2 that the sideline microphones compare very favourably between the snapshot arrays and traditional linear array, with a deviation of only 0.1 SEL [dBA]. However, the centre microphone exhibits a 1.6 SEL [dBA] difference, which can be considered a large difference. The measured SEL from the centre microphones of each array was investigated, and it was found that the average SEL value for all runs was  $81.3 \pm 0.8$  dBA when scaled to the same flight altitude used in the model. This matches well with the traditional linear array but is not within the error of the snapshot arrays.

The difference between linear and snapshot arrays is concerning, especially since the snapshot array predictions do not align with the measured values for the centre microphones. There are two known errors that are likely complicating this analysis. The first error is that the microphone measurements are quite sparse for an individual snapshot array. The interpolation scheme used in the Acoustic Repropagation Technique linearly interpolates along frequency between azimuth and elevation angles (effectively), without regard to the aerodynamic phenomena which produces the acoustics. This linear interpolation is used heavily on the snapshot arrays where there are large areas between measurement points, but is less prominent on the traditional linear array due to the density of available data. This is easily seen by looking at the areas not covered in microphones for the snapshot array shown in Figure 5 compared to the linear array in Figure 6. Fortunately, this issue can be mollified in future work by using the FRAME technique to create hemispheres that are semiempirically predicted to fill the missing areas instead of linearly interpolated<sup>[6]</sup>. It is also possible on future arrays to add microphones in directions most needed for land-use planning models, in this case additional microphones along the  $180^\circ$  azimuthal direction would have improved the comparison between modelled and measured data.

The second significant source of error that is likely

affecting the predictions is the high wind experienced during the experimental portion of the campaign. Typically, a wind cut-off is established at 10 knots, such that any winds above 10 knots results in the cessation of testing that day due to data quality concerns. Unfortunately, this test had winds in excess of such limits for the vast majority of the flights, and for all of the runs used in this paper. The affect of side winds on the tail rotor noise was a concern up front, and it is likely that this has contributed to the discrepancies seen here. The pilot also commented during testing that the wind direction changed somewhere around  $X = 200$  m and that he had to change the tail rotor condition to account for that change. Unfortunately, this change in direction is not captured by our single-location LIDAR measurement, and so no quantitative discussion can be made on the magnitude of the change. It is noted further that the winds affect acoustic propagation as well as the source noise, so it is also possible that the winds have modified the relative directivity from the hemisphere that was not accounted for in the straight-ray propagation used in the Advanced Acoustic Model. Future work will look at modelling each hemisphere individually and propagating it across the array with weather affects using the Wave Confinement method<sup>[28,29]</sup>.

## 5. CONCLUSIONS

A snapshot array measurement technique was developed to provide adequate hemispherical measurement coverage at a single instant in time. The intent of the snapshot array is to provide the capability to measure vehicles with unsteady acoustic emissions, like those expected in the complex configurations produced by the eVTOL community and for Future Vertical Lift vehicles. The desire is to be able to use such hemispheres with land-use planning models. The snapshot hemisphere design was tested, and it was shown to be capable of capturing unsteady acoustic emissions as seen by the variability among snapshot hemispheres.

The snapshot array hemispheres were compared to simultaneously captured linear array hemispheres, which are the traditional design for land-use planning models. The difference in A-weighted Sound Exposure Levels between the traditional hemispheres and snapshot hemispheres was interrogated for certification style microphones. Both sets of hemispheres were shown to compare favourably for receivers off to each side of the vehicle, with average values agreeing within 0.1 SEL [dBA]. However, underneath the flight track a large discrepancy of 1.6 dBA was noticed, and this was attributed to a combination of factors. Factors that affect the quality of hemisphere are the interpolation model used to create the hemisphere, as well as the multiple effects of excessive winds experienced during this experiment.

Future work will involve looking at using a semiempirical method to interpolate between measurement points, instead of the linear frequency weighting used in this paper. The effect of wind on acoustic propagation will also be evaluated in a future paper. Overall this method has proven to be a viable concept, but future refinements are required before it can be used with confidence on complex vehicles.

## References

- <sup>1</sup>Vail, E., "Adopt Local Law- Amending Chapter 75 (Airport) of the Town Code Regulating Nighttime Operation of Aircraft at East Hampton Airport," East Hampton Town Board Resolution 2015-411, 2015.
- <sup>2</sup>Uber, "Fast-Forwarding to a Future of On-Demand Urban Air Transportation," *White Paper*, 2016.
- <sup>3</sup>Vertical Flight Society, "Vertical Flight Society Electric VTOL Directory Hits 600 Concepts," *Press Release*, January 2022.
- <sup>4</sup>Pascioni, K. A., Watts, M. E., Houston, M. L., Lind, A. H., Stephenson, J. H., and Bain, J. J., "Acoustic Flight Test of the Joby Aviation Advanced Air Mobility Prototype Vehicle," *28<sup>th</sup> AIAA/CEAS Aeroacoustics Conference*, 2022.
- <sup>5</sup>Conner, D. and Page, J., "A Tool for Low Noise Procedures Design and Community Noise Impact Assessment: The Rotorcraft Noise Model (RNM)," *AIAA*, 2002.
- <sup>6</sup>Greenwood, E., *Fundamental Rotorcraft Acoustic Modeling from Experiments (FRAME)*, Ph.D. thesis, University of Maryland, 2011.
- <sup>7</sup>Greenwood, E., Schmitz, F. H., and Sickenberger, R. D., "A Semi-Empirical Noise Modeling Method for Helicopter Maneuvering Flight Conditions," Proceedings of the 68<sup>th</sup> Annual Forum of the American Helicopter Society, Ft. Worth, TX, May 2012.
- <sup>8</sup>Brentner, K. S. and Jones, H. E., "Noise Prediction for Maneuvering Rotorcraft," *6<sup>th</sup> AIAA/CEAS Aeroacoustics Conference*, 2000, AIAA 2000-2031.
- <sup>9</sup>Bres, G. A., Brentner, K. S., Perez, G., and Jones, H. E., "Maneuvering Rotorcraft Noise Prediction," *Journal of Sound and Vibration*, Vol. 275, 2004, pp. 719–738.
- <sup>10</sup>Spiegel, P., Buchholz, H., and Pott-Pollenske, M., "Highly instrumented BO-105 and EC135-FHS aeroacoustic flight tests including maneuver flights," Proceedings of the 61<sup>st</sup> Annual Forum of the American Helicopter Society, Grapevine, TX, May 2005.
- <sup>11</sup>Chen, H., Brentner, K. S., Lopes, L. V., and Horn, J. F., "An initial analysis of transient noise in rotorcraft maneuvering flight," *International Journal of Aeroacoustics*, Vol. 5, (2), 2006, pp. 109–138.
- <sup>12</sup>Schmitz, F. H., Greenwood, E., Sickenberger, R. D., Gopalan, G., Sim, B. W.-C., Conner, D., Moralez, E., and Decker, W. A., "Measurement and Characterization of Helicopter Noise in Steady-State and Maneuvering Flight," Proceedings of the 63<sup>rd</sup> Annual Forum of the American Helicopter Society, Virginia Beach, VA, May 2007.
- <sup>13</sup>Watts, M. E., Snider, R., Greenwood, E., and Baden, J., "Maneuver Acoustic Flight Test of the Bell 430 Helicopter," Proceedings of the 68<sup>th</sup> Annual Forum of the American Helicopter Society, Ft. Worth, TX, May 2012.
- <sup>14</sup>Watts, M. E., Greenwood, E., Sim, B., and Stephenson, J., "Helicopter Acoustic Flight Test with Altitude Variation and Maneuvers," Technical Memorandum NASA/TM-2016-219354, NASA Langley Research Center, Hampton, VA 23681, USA, December 2016.
- <sup>15</sup>Greenwood, E., "Helicopter Flight Procedures for Community Noise Reduction," Proceedings of the 73<sup>rd</sup> Annual Forum of the American Helicopter Society, Ft. Worth, TX, May 2017.
- <sup>16</sup>Watts, M. E., Greenwood, E., Smith, C., and Stephenson, J., "Noise Abatement Flight Test Data Report," Technical Memorandum NASA/TM-2019-220264, NASA Langley Research Center, Hampton, VA 23681, USA, March 2019.
- <sup>17</sup>Pascioni, K. A., Greenwood, E., Watts, M. E., Smith, C. D., and Stephenson, J. H., "Medium-Sized Helicopter Noise Abatement Flight Test Data Report," Technical Memorandum, NASA Langley Research Center, Hampton, VA 23681, USA, 2020.
- <sup>18</sup>Stephenson, J. H., Watts, M. E., Greenwood, E., and Pascioni, K. A., "Development and Validation of

Generic Maneuvering Flight Noise Abatement Guidance for Helicopters,” *Journal of the American Helicopter Society*, Vol. 67, (1), January 2022, pp. 1–12.

Annual Forum of the American Helicopter Society, Ft. Worth, TX, May 2017.

<sup>19</sup>Page, J. A., Plotkin, K. J., and Hobbs, C., “Acoustic Repropagation Technique Version 2 (ART2),” *Wyle Laboratories. Arlington: Wyle Laboratories*, 2001.

<sup>20</sup>Greenwood, E., Brentner, K. S., Rau, R. F., and Gan, Z. F. T., “Challenges and opportunities for low noise electric aircraft,” *International Journal of Aeroacoustics*, 2022, pp. 1–67.

<sup>21</sup>Stephenson, J. H., Watts, M. E., Greenwood, E., and Pascioni, K. A., “Development and Validation of Generic Maneuvering Flight Noise Abatement Guidance for Helicopters,” Proceedings of the 76<sup>th</sup> Annual Forum of the Vertical Flight Society, Virginia Beach, VA, October 2020.

<sup>22</sup>Page, J. A., Wilmer, C., Schultz, T., Plotkin, K. J., and Czech, J., “Advanced Acoustic Model Technical Reference and User Manual,” Technical report, WYLE LABS EL SEGUNDO CA, 2010.

<sup>23</sup>Stephenson, J. H., Lind, A., Hutchins, C., Pascioni, K., Houston, M., and Martin, P., “Yuma 2022 Rotorcraft Acoustic Flight Test,” Technical Memorandum NASA/TM-20220004483, NASA Langley Research Center, Hampton, VA 23681, USA, April 2022.

<sup>24</sup>“Ground-Plane Microphone Configuration for Propeller-Driven Light-Aircraft Noise Measurement,” ARP 4055, SAE, November 2007.

<sup>25</sup>Anderson, M. C., Stephenson, J. H., Zawodny, N. S., and Gee, K. L., “Characterizing the effects of two ground-based outdoor microphone configurations,” Proceedings of Meetings on Acoustics 178ASA, Vol. 39, 2019.

<sup>26</sup>Conner, D. A., Burley, C. L., and Smith, C. D., “Flight acoustic testing and data acquisition for the Rotor Noise Model (RNM),” Proceedings of the 62<sup>nd</sup> Annual Forum of the American Helicopter Society, Phoenix, AZ, May 2006.

<sup>27</sup>Shepard, D., “A two-dimensional interpolation function for irregularly-spaced data,” Proceedings of the 1968 23<sup>rd</sup> ACM national conference, 1968.

<sup>28</sup>Chitta, S., Steinhoff, J., Wilson, A., Caradonna, F., Sim, B., and Sankar, L., “A New Finite-Difference Method for General Long-Range Rotorcraft Acoustics: Initial Comparisons with Intermediate-Range Data,” *American Helicopter Society 70<sup>th</sup> Annual Forum*, 2014.

<sup>29</sup>Stephenson, J. H., Sim, B. W., Chitta, S., and Steinhoff, J., “Sound Diffraction Modeling of Rotorcraft Noise Around Terrain,” Proceedings of the 73<sup>rd</sup>